# Silicon Photonic Subsystem for Broadband and RoF Detection While Enabling Carrier Reuse

Mingyang Lyu, Wei Shi, and Leslie A. Rusch

OSA Optics Express, (Volume 28, Issue 10) (2020)

https://doi.org/10.1364/OE.391194

# Silicon Photonic Subsystem for Broadband and RoF Detection While Enabling Carrier Reuse

**MINGYANG LYU, WEI SHI, AND LESLIE A. RUSCH***

*Centre for Optics, Photonics, and Lasers (COPL), ECE department, Université Laval, Québec, QC G1V 0A6, Canada*
*rusch@gel.ulaval.ca

**Abstract:**
We experimentally validate a silicon photonic subsystem designed for passive optical networks with carrier reuse. The subsystem is intended for future wavelength division multiplexed (WDM) PONs. It enables radio-over-fiber signals to cohabit an assigned wavelength slot without perturbing the PON signal, and conserving carrier power for the uplink. A microring modulator remodulates the residual carrier for the RoF uplink. We successfully detected the dropped an 8 GHz broadband signal and five 125 MHz radio-over-fiber signals. Two 125 MHz radio over fiber signals are remodulated onto the carrier. The uplink signal shows good performance, validating the residual downlink signals have been well rejected by the microring filters. The subsystem conserves a clean carrier for remodulation with good signal-to-carrier ratio.



The rapid growth of mobile services and video streaming is driving requirements for greater bandwidth and higher quality communication services. Passive optical networks (PONs) provide low loss fiber transmission and silicon photonics can bring down the cost of transceiver technologies. Additional PON revenue streams can be created by supporting heterogeneous signals - both basic broadband network access and radio over fiber (RoF) signalling for 5G femtocells [1,2]. Expanded services must conserve features keeping costs low for PONs: colorless operation with carrier reuse and a single fiber structure (as opposed to a dual feeder) [3–5].

Silicon photonics can realize highly integrated, low cost and small footprint systems, attributes particularly attractive in the cost sensitive PON market [6, 7]. Though several companies already provide single-chip silicon photonics integrated circuits (PICs) that include all transmit and receive functions, those solutions typically employ coherent detection and incorporate co-packaged laser sources. A PON solution should avoid lasers to lower cost and maintain colorless transceivers.

We propose an integrated transceiver solution for PON with carrier reuse. The demonstrated ONU subsystem is designed for the optical line terminal (OLT) supporting 1) the hybrid direct detection of broadband signals and RoF signals within the same wavelength slot, as well as 2) the remodulation of the carrier for the uplink signal. Cascaded microring resonators (MRRs) assure the isolation of received RoF and broadband signals from one another; they also work as routing components, further decreasing system complexity. Separate on-chip photodetectors (PDs) provide the simultaneous detection of RoF and broadband signals. The MRRs leach off the minimum carrier power needed for each detection, and suppress downlink signals to leave the residual carrier free for remodulation via an on-chip microring modulator (MRM). In our experiment we do a proof of concept with RoF signals of various widths and placement to examine the feasibility of SiP resonant structures for this application. To support the RoF signals, we create a SSB OFDM signal with guard band, where the RoF signals are transmitted.

Direct detected single sideband OFDM (DD-SSB OFDM) with carrier reuse is a promising solution for next generation PONs. It is particularly flexible in sculpting both time and frequency resources [8], and uses low cost direct detection. To avoid fading induced by chromatic dispersion [9], single side-band OFDM is employed. Our demonstrations assume DD-SSB

National Science and Engineering Research Council of Canada (NSERC) Funding: CRDPJ 499664

OFDM, but are equally valid for other broadband modulation formats.

The paper is organized as follows. We first discuss the details of the fabricated OLT subsystem in section 1. In section 2 we explain the experimental setup in detail. In section 3 we focus on the hybrid detection section of the OLT subsystem. After discussing the design and characterization of the two sets of cascaded MRRs, we examine the downlink performance of RoF and OFDM experimentally. In section 4 we first explain the design and characterization of the MRM to be used for RoF uplink via remodulation of the downlink carrier. The performance of the MRM modulated RoF uplink is evaluated experimentally, with and without the downlink detection in place. Finally, some concluding remarks are made.

## 1. Subsystem Design

The subsystem architecture and operating principle are illustrated in Fig. 1. The upper section shows the PIC with two stages of cascaded pairs of MRRs and a final stage of an MRM. The notations (A), (B) and (C) located near MRR set1, MRR set2 and the MRM, respectively, indicate reference probe points for input spectra. The lower section shows a cartoon of the optical spectrum as signals propagate through the subsystem. The input spectrum has a red block to represent the OFDM (basic broadband network access) signal; the black arrow is the optical carrier. The guard band between the carrier and OFDM signal contains a narrowband RoF signal represented by a narrow black block. As the guard band is as wide as the OFDM signal, signal to signal beating interference (SSBI) can be eliminated in the electrical domain by a bandpass filter over the OFDM signal.

Consider the spectrum marked (A) in the lower section of Fig. 1. The first pair of cascaded MRRs (MRR set1 drawn as orange ovals, with its drop port passband sketched in orange dotted lines below) will drop the RoF signal. The MRR is tuned to cut only enough carrier power for RoF detection. The through path sees the RoF signal suppressed.

Consider next the spectrum marked (B) in the lower section of Fig. 1. The signal with suppressed RoF enters the second pair of cascaded MRRs (MRR set2 drawn as green ovals, with its drop port pass band sketched in green dotted lines below). The second cascade drops the OFDM signal, again cutting just enough of the optical carrier for direct detection. Both cascaded MRRs are thermally tuned via metal deposits to adjust their resonance peak distance, extinction ratio and central wavelength. The two MRR sets are tuned individually.

Referring finally to the spectrum marked (C) in the lower section of Fig. 1, the final stage remodulates the carrier with uplink RoF signals. The blue blocks to either side of the carrier and superimposed on the residual RoF downlink represent the output of the MRM.

The RoF signals are dropped firstly to an on-chip PD. The OFDM signal and most carrier power pass through the first MRR set. We tune these MRRs to confine their response to cover the narrowband RoF signals, avoiding undesired filtering of the carrier and OFDM signal. Only a very low level of the OFDM signal is dropped at the first MRM set, avoiding SSBI induced degradation of RoF detection.

The second MRR set sees the residual downlink RoF signal and lightly attenuated downlink OFDM signal and carrier. As shown in spectrum (B), we drop the OFDM signal and a part of the carrier to a second on-chip PD. A more shallow response is required from these MRRs to cover the wideband OFDM signal. The large guard band ensures SSBI is out-of-band for OFDM detection. In the absence of SSBI, we can reserve most carrier power for the uplink.

The final sketch of the spectrum (C) shows our strategy of suppression of the downlink signals by the MRR stages, and uplink RoF generation. The uplink can exploit spectrum on either side of the carrier if needed. An IQ modulator could be used to generate a single sided RoF signal if preferred. Note that the RoF signals are represented as a single block, but may have multiple narrowband signals (for multiple antennas, for instance) within that pass-band.

While our experiment shows the uplink exiting a separate port, in future designs the remodulated

National Science and Engineering Research Council of Canada (NSERC) Funding: CRDPJ 499664

signal could be guided through another optical path for a true single feeder structure. For instance, a reflective structure could be added to the MRM output to send the uplink signal back along the same path. The MRR filtering would then allow single sideband modulation without an IQ MRM. The MRM double sided uplink signal would see the left sideband filtered by the cascaded MRR sets, while the right sideband would remain (mostly) unchanged. As the dropped left sideband of the uplink signal would be guided to a different MRR port than the one connected to the PDs, the downlink detection would not be perturbed.

Since silicon photonics is based on high-index-contrast waveguides compatible with CMOS technology, high speed optical modulators [10] could be realized along side the common passive components. Figure 1 shows the transceiver subsystem layout we sent for fabrication. The ultra small footprint and low power consumption (down to Fj/bit), of the MRM lowers overall cost. The total footprint of our proof-of-concept subsystem is 0.5 mm × 1.475 mm, dominated by the bond pads for DC and RF probes. The blue shaded pads are for DC connections for thermal tuning. The red shaded pads are for RF probes to 1) capture the detected downlink signal and 2) carry the RF uplink signal for remodulation of the carrier. The ability to tune the wavelengths of the MRRs and MRMs makes our subsystem compatible with WDM PONs [11].

## 2. Experimental Setup

The experimental setup is illustrated in Fig. 2. A Cobrite external cavity laser source with 100 kHz linewidth is split via a 3-dB coupler. One of the coupler output ports is connected to an SHF IQ modulator to generate the SSB downlink signal; the IQ modulator is biased at the null point to suppress the carrier in this branch. The other coupler output is used as the distributed carrier, with a variable optical attenuator (VOA) to adjust signal-to-carrier ratio.

The RoF and OFDM downlink signals (both QPSK) are generated offline with Matlab and sent to a digital to analog converter (DAC). The FFT size is 1024, covering 64 GHz (DAC sampling rate is 64 GS/s). The wideband OFDM signal includes 127 subcarriers, occupying just

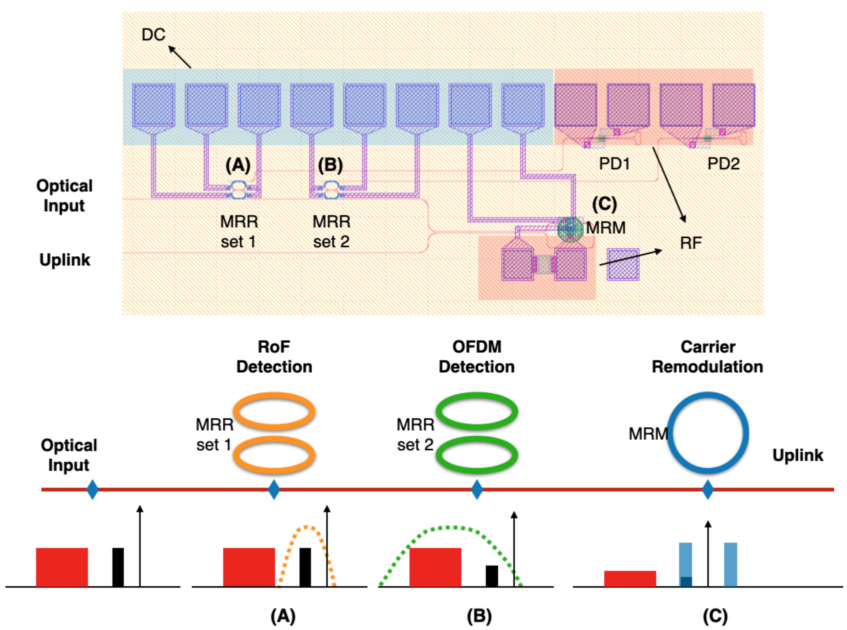


Fig. 1. Principle of operation of the SiP subsystem. MRR drop ports are not shown.

National Science and Engineering Research Council of Canada (NSERC) Funding: CRDPJ 499664

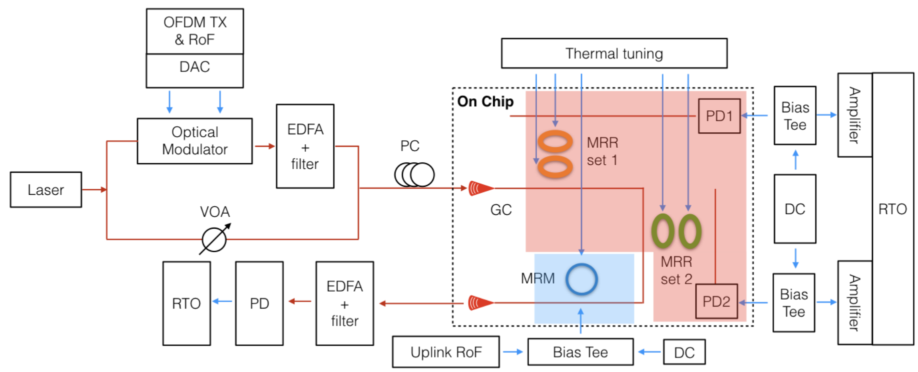


Fig. 2. Experimental setup to test subsystem.

under 8 GHz, with an 8 GHz guard band. The complex coordinates of single sideband (SSB) OFDM are generated using two 8-bit DAC channels. The net bit rate for broadband SSB-OFDM transmission is 16 Gb/s and we use direct detection. The narrowband RoF signal is made from five 125 MHz RF signals spaced at 250 MHz and occupying a total bandwidth of 2 GHz within the guard band.

Clipping (5 dB peak-to-average threshold) and pre-compensation are used to compensate the limited dynamic range and bandwidth of the DAC, particularly in the presence of OFDM high peak-to-average power ratio. An Inphi amplifier amplifies the DAC output. The SHF IQ modulator generates the optical SSB signal that is amplified by an erbium doped fiber amplifier (EDFA) and then filtered by a 0.7 nm bandpass filter to suppress amplified spontaneous emission from the EDFA.

The downlink signal is coupled into the chip via a 250 $\mu$m spaced fiber array. A polarization controller is used before coupling as the grating couplers (GCs) are polarization sensitive. Our choice of the polarization-sensitive grating coupler for experimental convenience required us to include a polarization controller before coupling. A second generation of the subsystem would use an edge coupler with no polarization sensitivity, and greatly reduce coupler loss.

The integrated subsystem (on-chip portion) is demarcated by the dotted rectangle. The red shading shows the sections for downlink detection, while blue shading is for uplink generation. The downlink detection section includes two sets of cascaded MRRs and two on-chip PDs. Each MRR set drops the desired signal (RoF or OFDM) to the PD. The four MRRs are thermally controlled to achieve the desired frequency response shape. The PDs are reverse-biased with 3V via bias-tees. The electrical signals are amplified and captured by a real-time-oscilloscope (RTO) with a 40 GS/s sampling rate and a 32 GHz RF front end via the RF probe.

The uplink section is a p-i-n based MRM to remodulate the residual carrier. A separate DAC output is used for the uplink RoF signal; it is amplified and probed onto the MRM. The MRM wavelength is thermally tuned to match the residual carrier. The remodulated uplink signal is coupled out of the chip via the fiber array and then amplified by an EDFA. An off-chip PD with a transimpedance amplifier is used to detect the RoF uplink signal that is captured on a separate RTO channel and processed offline with standard digital signal processing (DSP).

National Science and Engineering Research Council of Canada (NSERC) Funding: CRDPJ 499664

## 3. Hybrid Broadband and RoF detection

### 3.1. Characterization of cascaded MRRs

We use two MRR cascaded pairs with similar designs to drop the downlink RoF and OFDM signals. The layout of a cascaded MRR pair with a symmetric structure is shown in Fig. 3(a). The ring radii are 10 $\mu$m; a 13 $\mu$m linear waveguide introduced into the rings creates oval structures, resulting in free space range (FSR) around 6 nm. The gap between the rings and the waveguide is 210 nm, while there is a 315 nm gap between the two rings. These gaps are the only difference between the MRR sets. The first MRR set requires very sharp notch shape response to drop the narrowband RoF signal and a part of the carrier power. To drop the wide band OFDM signals, the second MRR has a gap between the rings and the waveguide of 200 nm, and a gap between the two rings of 305 nm. The smaller gap gives higher coupling efficiency, yielding a more shallow response to cover a wider frequency range.

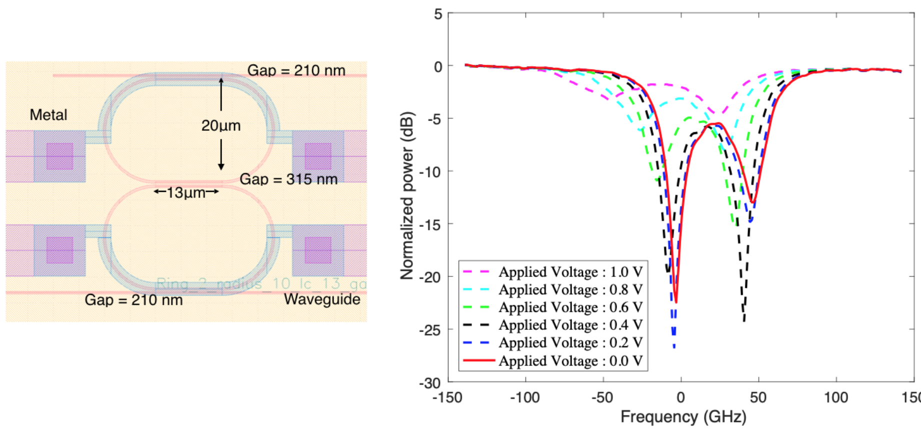


(a) (b)

Fig. 3. (a) Mask layout of MRR set1; (b) MRR responses with thermal tuning

Fig. 3(b) shows the cascaded MRR through port response (red solid curve) and the responses (dotted curves) when sweeping the voltage on one of the two heaters. By applying different voltages to each heater, we could control the red shift of the response and move the response peak to the desired frequency. More importantly, by heating the two rings in the cascade independently, we could change the overall response from sharp notches (extinction ratio more than 25 dB) to a shallow shape. This allows us to control the carrier power dropped, and to select the component of the downlink signal to route to the photodetector. The resonance peaks from the two constituent MRRs in the cascade are spaced by more than 50 GHz, large enough to ensure the signal is filtered by only one notch.

### 3.2. Hybrid Broadband and RoF detection

Figure 4 shows the optical spectrum at three different points in the red shaded portion of Fig. 2. The spectrum of the signal at the chip input is given in black. We see the carrier at 1557.03 nm, the five separate RoF signals directly to the left, and finally the 8 GHz wide SSB-OFDM signal farther to the left at the end of the guard band. The frequency responses of two MRR sets, $H(f)_{MRRset1}$ and $H(f)_{MRRset2}$, are sketched in dotted orange and green lines, respectively. An inset zooms in on the carrier to show how much of carrier power is dropped at various points along the chip.

National Science and Engineering Research Council of Canada (NSERC) Funding: CRDPJ 499664

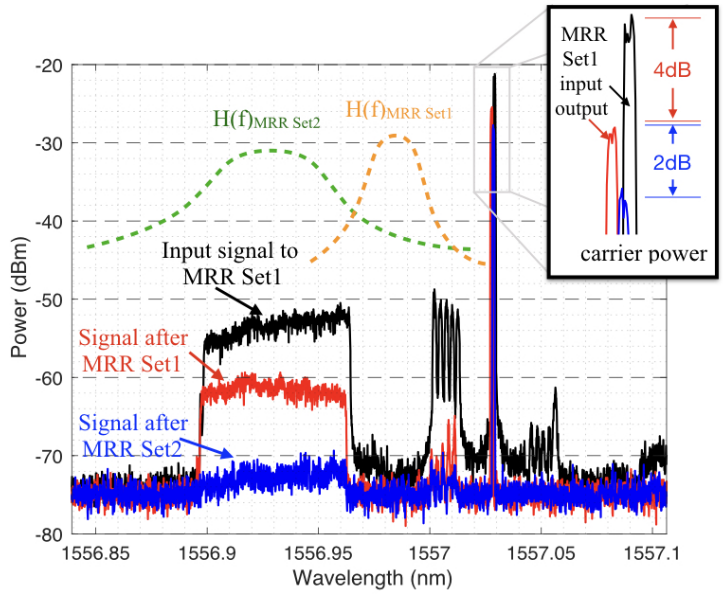


Fig. 4. Optical spectrum at three measurement points: black curve is input to chip, red curve is output of MRR set 1, blue curve is output of MRR set 2; frequency responses of each set of cascaded MRRs are sketched in dotted lines; an inset zooms on the carrier to show carrier power dropped by MRRs.

### *3.3. RoF detection*

The two rings in the cascade are tuned to achieve critical coupling, thus creating a very narrow and deep notch in the through port. The notch is centered on the RoF signal to minimize its residual going to the next section. The dotted orange curve in Fig. 4 above the five RoF signals labeled $H(f)_{MRRset1}$ is the approximate drop port frequency response of the first set of MRRs. We drop a small portion of carrier and the entire RoF signal to the PD. The tuning was used to maximize RoF detection with minimal attenuation of the OFDM signal. The amount of carrier dropped could also be adjusted in this manner. As silicon photonics cannot yet offer mature on-chip amplification, preservation of carrier power is important to enable this integrated solution for uplink transmission. The resonance peak of MRR set1 is tuned slightly away from the carrier to let more carrier power pass the MRR set1 at the sacrifice of the downlink signal detection performance.

The red curve in Fig. 4 shows the spectrum after the RoF signal is dropped, i.e., the signal entering the second set of cascaded MRMs. We observe around 20 dB suppression of the RoF signal. To combat the anticipated filtering effect of MRR set1 on the OFDM signal, additional power was assigned to the first subcarriers of OFDM signals (see upward tilt in black curve in Fig. 4), i.e., a form of pre-emphasis. With this precaution, there is little degradation of the OFDM signal; the red OFDM sprectrum is flat. We see in the inset that the carrier power was reduced by only 4 dB, sufficient for RoF reception.

The photodetected electrical spectrum of the RoF signal is given in Fig. 5(a). We set the RTO built-in low pass filter to 8 GHz and capture the detected signal at 20 GS/s. An attenuated version of the OFDM signal is dropped (the lowest frequency subcarriers are visible in the electrical spectrum). The residual OFDM results in interference at base band (lower than 1 GHz). The five RoF signals at 2 GHz are unaffected by this interference that can be easily filtered out. To reflect

National Science and Engineering Research Council of Canada (NSERC) Funding: CRDPJ 499664

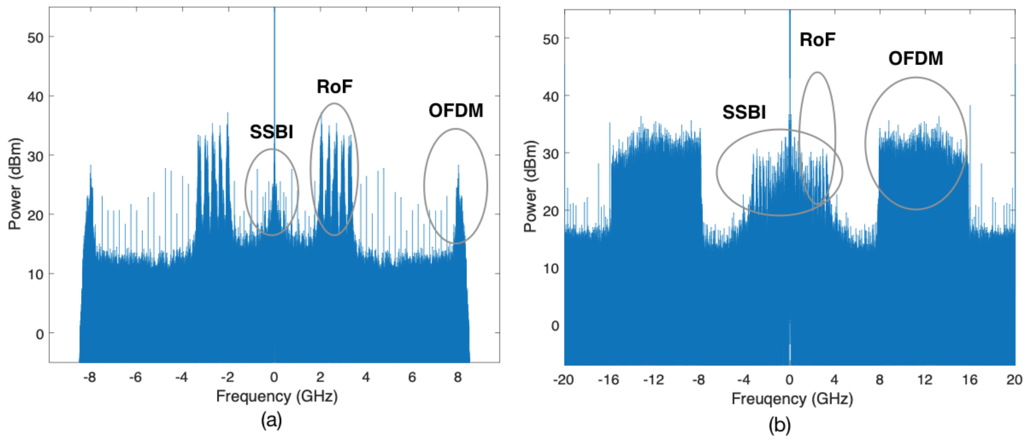


Fig. 5. Electrical spectrum of detection of (a) RoF signal, (b) OFDM signal.

the nature of a 5G receiver, the captured RF signal are down-sampled to 8 GS/s and digitally filtered to separate the five RoF channels. Only a small FFT size (128) is needed. For all five channels the bit error rate (BER) is well under the forward error correction (FEC) threshold. The Q-factor calculated from measured BER of the five RoF channels is 9.57 dB, 10.51 dB, 11.71 dB, 10.88 dB, 11.85 dB from low to high frequency.

### *3.4. Broadband detection*

The strategy for OFDM detection is simple. As illustrated by the green dotted line in Fig. 4, we tune the second set of MRRs to a shallow shape to allow a wide, flat pass-band for OFDM. The resonance peak is slightly tuned away the carrier instead of falling on the center of OFDM signal band, allowing lower dropped carrier power. The blue curve in Fig. 4 shows the optical spectrum at the output of the OFDM drop stage, i.e., after MRR set 2. The downlink OFDM signal is well suppressed, and the carrier power has only decreased by 2 dB. The OFDM signal is captured by the RTO at 40 GS/s and 32 GHz electrical bandwidth. The normal FFT size (1024) is used. The photodetected electrical spectrum of the OFDM signal is given in Fig. 5(b). The SSBI falls into the guard band, as well as residual RoF. The BER is $3.2\times10^{-3}$, below the 7% FEC threshold.

## 4. Carrier Reuse

### *4.1. Characterization of MRM*

Figure 6(a) shows the partial mask layout including the MRM; a zoom shows the p-i-n structured MRM. The MRM has diameter of 20 $\mu$m, and a gap between the ring and waveguide of 300 nm. In contrast to the other silicon based modulators, our choice of carrier injection based p-i-n modulator provides higher modulation depth and larger changes of refraction index in micron-size footprint [12]. Though the bandwidth of the p-i-n modulator is limited due to the slower diffusion of minority carriers, the low swing voltage [13, 14] is still attractive for OLT applications.

The cross section of the MRM is illustrated in Fig. 6(b). Highly doped P (P++, P+ ) and N regions (N++, N+ ) are separated by the intrinsic region formed by the waveguide. The waveguide width is 500 nm while the gaps between the P+/N+ region and waveguide are 250 nm and 500 nm respectively.

The measured optical transmission spectra of the MRM for various bias voltages are presented in Fig. 6(c). The pink curve with triangle markers shows the spectrum with forward bias (0.75 V)

National Science and Engineering Research Council of Canada (NSERC) Funding: CRDPJ 499664

on the p-i-n junction. The bias voltage is still lower than the built-in potential of the junction. The spectrum shows a resonance depth of around 9 dB at 1557.15 nm. As the forward bias voltage increases, the electron-hole pair density in the cavity increases. Significant blue shifts are observed with larger bias voltage. The MRM is designed in the over-coupling region. Though the increasing electrons and holes result in stronger optical absorption, the depths of the notches are increased due to the lower effective index. The MRM is forward biased at 0.85 V in our experiments.

### 4.2. Remodulation results

We examine the remodulation of the carrier by an uplink RoF signal with two RF sub-components one at 2.25 GHz from the carrier and the other at 2.625 GHz. The limited bandwidth of the p-i-n structured MRM leads to the 2.625 GHz signal having poorer performance; we therefore apply pre-emphasis. We inject a pure carrier into the chip to find the appropriate pre-emphasis and confirm similar performance without downlink signals present.

To examine the impact of residual downlink signals on uplink RoF, we have carefully chosen the uplink RoF signal location. Figure 7 illustrates the uplink signal allocations as well as the downlink RoF signals. The hashed, red rectangles represent the downlink RoF signals described previously: five 125 MHz RoF signals over 2 GHz with 250 MHz spacing. The solid blue blocks are the uplink signals, two 125 MHz RoF signals located at 2.25 GHz and 2.625 GHz from the carrier. This choice ensures that one uplink RoF channel is free from residual downlink RoF signals, while the other uplink RoF channel is totally overlapping a downlink RoF signal.

Consider first the pre-emphasized RoF uplink on a distributed carrier when no downlink signal is present. We accomplish this on our chip with DC voltages applied on the MRRs to tune the responses out-of-band. Hence we will see only the losses, but no filtering effects from the two MRR sets.

Next we add the downlink RoF and OFDM signals to the distributed carrier at the input of the MRM. To suppress the downlink signals, we set the DC voltages on the MRR heaters back to the values we used for RoF detection and OFDM detection. The MRR pairs drop the downlink RoF

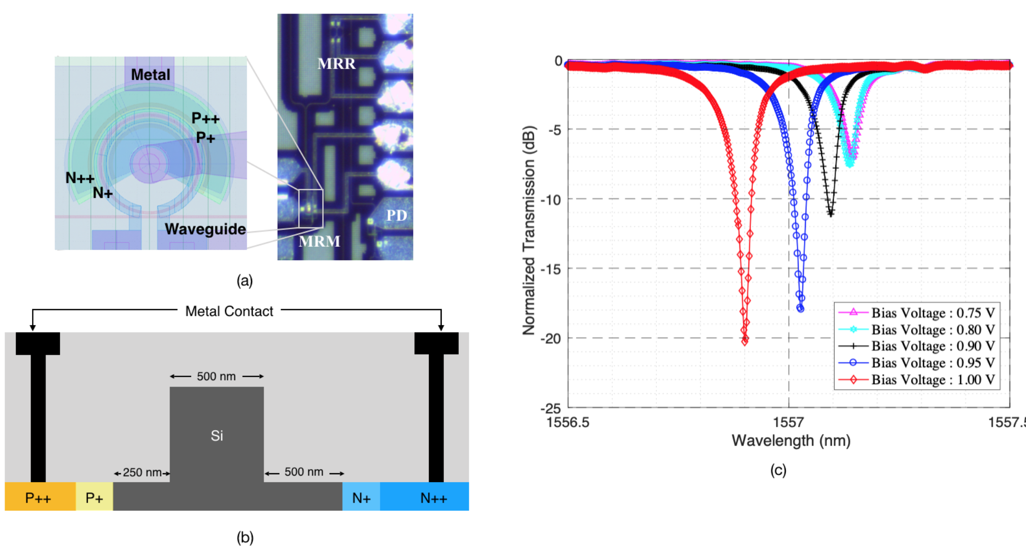


Fig. 6. MRM (a) partial mask layout, (b) cross section showing relevant dimensions, and (c) measured power transmission spectra at different bias voltages.

National Science and Engineering Research Council of Canada (NSERC) Funding: CRDPJ 499664

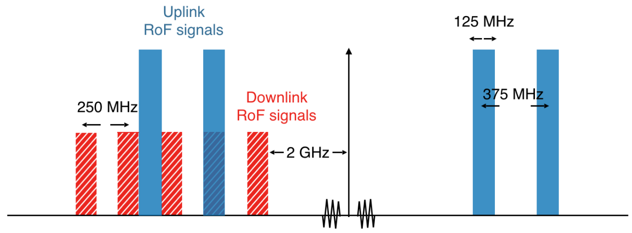


Fig. 7. Uplink RoF signals with downlink RoF signals

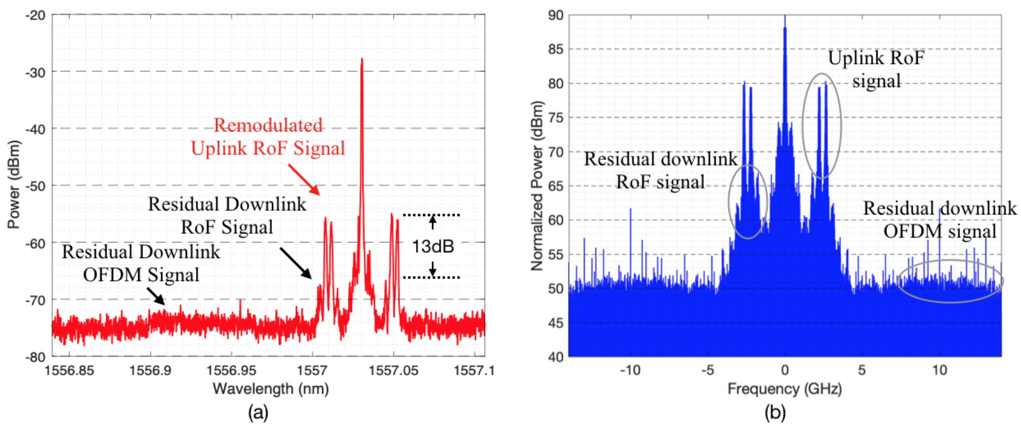


Fig. 8. Remodulated uplink signal (a) optical spectrum and (b) electrical spectrum

and OFDM signals and leave a clean carrier for remodulation.

Figure 8 shows the optical spectrum of the remodulated uplink signal as well as the residual downlink signal under this scenario. The resonance peak of the MRM is tuned to the carrier location. After proper pre-emphasis of the DAC output for the uplink RF signals, two uplink RoF channels with similar power are generated by remodulating the carrier. The downlink signals are well-suppressed by the subsystem, with residual RoF and OFDM signals with limited power observed in Fig. 8(a). The generated uplink RoF signal is 13 dB over the downlink signals, indicating their robustness against the crosstalk from residual downlink signals.

The modulated uplink signal is coupled out of chip via the fiber array. The light is amplified by an EDFA and passes through a 0.7 nm optical filter before photodetection. The directly detected electrical signal is captured by the RTO. We count errors and infer the Q-factor from the measured BER.

The direct detection uplink signal faces possible impairment from residual downlink signals. The residual downlink RoF signal could cause direct, in-band crosstalk to the uplink. The residual OFDM signal, while out-of-band, could lead to SSBI covering the whole guard band including the RoF uplink. Figure 8(b) presents the electrical spectrum at the uplink receiver. The downlink OFDM signal and the RoF signals both receive significant suppression. Two uplink RoF signals can be distinguished from the residual downlink RoF signals.

As there is good suppression of the downlink signal, there is no appreciable SSBI. The good suppression of the downlink RoF signals leads to little impairment in the uplink signal. The calculated Q-factors for the two uplink RoF signals are 13.77 dB and 14.12 dB, which confirms

National Science and Engineering Research Council of Canada (NSERC) Funding: CRDPJ 499664

hybrid detection is compatible with providing the carrier reuse for uplink signal modulation.

### *4.3. Discussion*

This work is a proof of concept of SiP-based direct detection transceiver. The power budget is the main limiting factor in our experiment. The round trip coupling loss is large (13 dB), however this could be reduced to less than 3 dB with mature commercial packaging.

To simplify the experiment, our OFDM signal had a guard band as wide as the signal bandwidth (8 GHz). The guard band could be reduced to improve spectral efficiency, leaving only sufficient bandwidth for the RoF signals. Considering an RoF signal at 2 GHz, a 4 GHz guard band would be sufficient spacing between the downlink signal and RoF signal. The spectral efficiency would be increased from 0.5 to 0.75. With more precise filtering, the guard band could be further decreased. For instance, higher order ring structures have been shown to work well as re-configurable filters. As discussed previously, the detected RoF signal degradation is induced by residual broadband signal intended for the drop port.

Once the specific system parameters are set, we could determine an appropriate trade-off of the uplink carrier power and the residual downlink signal. In our proof of concept, we did not optimize the power assignment. The performance requirement for downlink and uplink transmission would determine the final strategy for the power budget. For example, in a transceiver the transmitter typically requires 70% of laser power. In our system, this would mean reserving 70% of the received carrier for remodulation, with the residual going to signal reception. We used 6 dB (75%) of the carrier for detection. The detection of RoF signal contributed to 4 dB carrier attenuation, i.e., even higher than OFDM detection. We could reduce RoF carrier requirements by about 2 dB by implementing a higher order MRR. Depending on uplink signal performance requirements, we could further decrease the carrier power for detection. Note that in a PON, the uplink could benefit from the greater sensitivity of coherent detection at the central office where laser sources are available. Hence, for a PON with a colorless ONU, the allocation of greater power resources to reception could be manageable.

We note the downlink signal in Fig. 4 shows greater suppression of the dropped RoF signal than we see after remodulation in Fig. 8; the difference is about 2 dB. The very limited bandwidth of the p-i-n modulator also induces some nonlinear distortion near the carrier, leading to some undesired out-of-band components. The slightly stronger residual RoF signals could be the result of thermal crosstalk. We apply a 4V voltage to the MRM heater, which heats the MRR pairs and causes a shift in the passband.

To address both thermal crosstalk and fabrication variations in the ring resonator, a feedback loop could be added to future subsystems. Due to the sensitivity of SiP components, automatic feedback control loop is generally required for commercial SiP products. For example, precise heating on ring resonators is demonstrated in [15]. Though ring-based structures are more vulnerable to temperature changes, they are still attractive for their ultra compact size and routing functions.

An automatic feedback control loop could be easily incorporated into our SiP structure, as illustrated in Fig. 9. A directional coupler guides a small portion of the RoF drop port to a monitor PD. The feedback loop must match the passband of the ring resonator to the RoF signal. The dropped signal has RoF as well as SSBI from the RoF signal, as sketched above the DC block element. The power of the detected RoF signal (black shaded rectangle) is determined by the dropped RoF and carrier power. The SSBI (grey shaded triangle) is determined on by the dropped RoF signal power. By monitoring the SSBI signal power, the passband of the rings could be tuned to the RoF signals. The SSBI signal could be monitored easily by using a low rate ADC with a lowpass response rejecting the RoF signal.

Our all-silicon solution cannot take advantage of on-chip amplification. Therefore our proposed subsystem husbands the carrier power; it has the downlink signal dropped via MRR

National Science and Engineering Research Council of Canada (NSERC) Funding: CRDPJ 499664

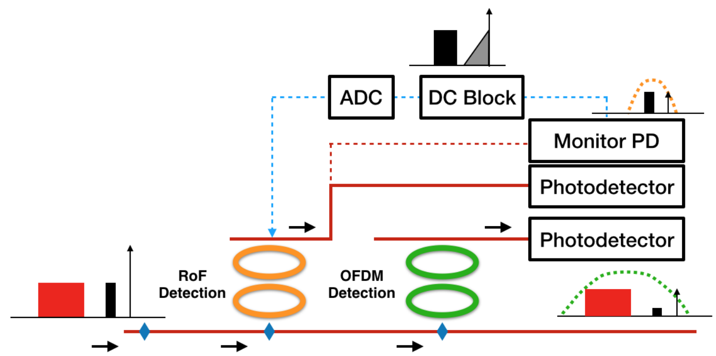


Fig. 9. Automatic Ring Control

pairs for detection and avoids splitters. By designing the MRR with higher quality factor, better separation of the carrier and downlink signal could be realized to improve the downlink detection performance and the uplink remodulation simultaneously.

## 5. Conclusion

We have proposed a novel silicon photonics subsystem supporting detection of RoF signals as well as the principle broadband signal. The proposed subsystem enables heterogeneous services and conserves carrier power to enable remodulation of uplink RF signals within a single feeder PON architecture. The subsystem is fabricated and experimentally validated. Five 125 MHz RoF signals and one 7.75 GHz OFDM downlink signal are detected simultaneously on-chip. Two 125 MHz RoF signals are generated by reusing the carrier via an on-chip MRM. The performance degradation on the uplink RoF signal induced by residual RoF downlink signal is only on the order of one half dB.

## Funding

This work is supported by research grants from Fonds de Recherche du Québec-Nature et Technologies (FRQNT) (2016-NC-190737), National Science and Engineering Research Council of Canada (NSERC) (CRDPJ499664), PROMPT Québec grant (52_Rusch 2016.09), TELUS, and Aeponyx. CMC Microsystems provided a subsidy for their fabrication and multi-project wafer service.

## Disclosures

The authors declare no conflicts of interest.

## References

1. K. Laraqui, "Small cell optical mobile backhauling: Architectures, challenges, and solutions," in *39th European Conference and Exhibition on Optical Communication (ECOC 2013),* (IET, 2013), pp. 1–3.
2. J.-i. Kani, F. Bourgart, A. Cui, A. Rafel, M. Campbell, R. Davey, and S. Rodrigues, "Next-generation pon-part i: Technology roadmap and general requirements," IEEE Commun. Mag. **47**, 43–49 (2009).
3. C. Chow, C. Yeh, C. Wang, F. Shih, and S. Chi, "Signal remodulation of ofdm-qam for long reach carrier distributed passive optical networks," IEEE Photonics Technol. Lett. **21**, 715–717 (2009).
4. J. Yu, O. Akanbi, Y. Luo, L. Zong, T. Wang, Z. Jia, and G.-K. Chang, "Demonstration of a novel wdm passive optical network architecture with source-free optical network units," IEEE Photonics Technol. Lett. **19**, 571–573 (2007).
5. Z. Jia, J. Yu, G. Ellinas, and G.-K. Chang, "Key enabling technologies for optical–wireless networks: optical millimeter-wave generation, wavelength reuse, and architecture," J. Light. Technol. **25**, 3452–3471 (2007).
6. A. Rickman, "The commercialization of silicon photonics," Nat. Photonics **8**, 579 (2014).

7. B. Charbonnier, S. Menezo, P. O'Brien, A. Lebreton, J. Fedeli, and B. B. Bakir, "Silicon photonics for next generation fdm/fdma pon," J. Opt. Commun. Netw. **4**, A29–A37 (2012).
8. N. Cvijetic, "Ofdm for next-generation optical access networks," J. lightwave technology **30**, 384–398 (2011).
9. J. Yu, M.-F. Huang, D. Qian, L. Chen, and G.-K. Chang, "Centralized lightwave wdm-pon employing 16-qam intensity modulated ofdm downstream and ook modulated upstream signals," IEEE Photonics Technol. Lett. **20**, 1545–1547 (2008).
10. W. Shi, Y. Xu, H. Sepehrian, S. LaRochelle, and L. A. Rusch, "Silicon photonic modulators for pam transmissions," J. Opt. **20**, 083002 (2018).
11. P. Dong, R. Shafiiha, S. Liao, H. Liang, N.-N. Feng, D. Feng, G. Li, X. Zheng, A. V. Krishnamoorthy, and M. Asghari, "Wavelength-tunable silicon microring modulator," Opt. express **18**, 10941–10946 (2010).
12. Q. Xu, S. Manipatruni, B. Schmidt, J. Shakya, and M. Lipson, "12.5 gbit/s carrier-injection-based silicon micro-ring silicon modulators," Opt. express **15**, 430–436 (2007).
13. S. Manipatruni, K. Preston, L. Chen, and M. Lipson, "Ultra-low voltage, ultra-small mode volume silicon microring modulator," Opt. express **18**, 18235–18242 (2010).
14. G. T. Reed, G. Mashanovich, F. Y. Gardes, and D. Thomson, "Silicon optical modulators," Nat. photonics **4**, 518 (2010).
15. W. S. Fegadolli, G. Vargas, X. Wang, F. Valini, L. A. Barea, J. E. Oliveira, N. Frateschi, A. Scherer, V. R. Almeida, and R. R. Panepucci, "Reconfigurable silicon thermo-optical ring resonator switch based on vernier effect control," Opt. express **20**, 14722–14733 (2012).

National Science and Engineering Research Council of Canada (NSERC) Funding: CRDPJ 499664